

ACOUSTO-ELECTRIC INTERACTION IN GaAs/AlAs SUPERLATTICE
USING SEPARATE-MEDIUM CONFIGURATION

M. Tabib-Azar

Elec. Engrg. and Applied Physics Dept.
Case Western Reserve University
Cleveland, Ohio 44106

M. N. Abedin and P. Das

Elec., Comp., and Systems Engrg. Dept.
Rensselaer Polytechnic Institute
Troy, New York 12180-3590

ABSTRACT

The acousto-electric interaction in GaAs/AlAs superlattice is studied using separate medium configuration. The transverse and longitudinal acousto-electric voltages (TAV and LAV) as a function of surface acoustic wave (SAW) frequency, temperature and incident photon energy are obtained. The magnitude and polarity of TAV and LAV exhibit strong SAW frequency ($\Delta f \approx 10$ KHz) dependencies. Also, the TAV spectrum exhibits structures at above GaAs bandgap photon energies. These are not observed in homogeneous semiconductors. SAW frequency dependence of TAV and LAV is attributed to generation of elastic waves in the superlattice. Structures in the TAV spectrum are attributed to electronic transitions among valence band and conduction band sub-levels in the quantum wells. Preliminary studies indicate that convolution signals also depend on SAW frequency. The experimental results with their explanation are presented and implication of these results in SAW based devices and SAW nondestructive characterization of superlattices is discussed.

I. Introduction

In recent years, new electronic phenomena have been demonstrated with structures that contain two-dimensional electron and hole systems (2DES and 2DHS). The majority of these phenomena are based on quantum confinement of carriers in an undoped region where, due to lack of ionized impurity scattering, high carrier mobilities are achievable. They are also based on the tunneling of the carriers through these quantum wells where their energies are quantized in the third dimension.

High carrier mobilities are required in constructing very high speed, low power transistors and logic circuits [1] and the tunneling phenomena is employed in a variety of devices such as ultrahigh frequency oscillators [2], tunable light detectors [3] and multiple level logic elements [4]. The quantization of the energy of the carriers is used in fabrication of high frequency optical modulators [5], using Stark effect, and optical logic elements [6] using enhanced excitonic effects. Also, record low-threshold laser operation has been demonstrated using recombination of quantum well confined electrons and holes [7]. The integration of these devices in a single chip to perform real time signal processing with blinding speed, near that of light, and higher bandwidth in the optical region

is not far away.

The surface acoustic wave (SAW) and semiconductor interaction has been used to build real time convolvers [8], imaging devices [9], with signal processing capability, and acoustic charge transport (ACT) [10] devices. The SAW technique has also been used in nondestructive characterization of semiconductors [11]. The possibility of tailoring the electrical properties of semiconductor structures using molecular beam epitaxy (MBE) and metal organic chemical vapor deposition (MOCVD) techniques has already led to the fabrication of more efficient ACT devices [10]. Experimentally, it is shown that the complete quantization of a 2DES in a strong magnetic field at low temperatures causes giant oscillation in the SAW attenuation [12].

Here we report experimental investigation of the behavior of the acoustoelectric voltages and convolution signals in GaAs/AlAs superlattices as a function of external excitations. We believe that the interesting properties of this interaction can be used as a basis for SAW based devices and non-destructive characterization of superlattices.

II. Experimental Procedure and Results

The experimental setup is shown in Fig. 1. The piezoelectric delay line is a y cut z propagating, highly polished LiNbO₃ where the surface acoustic wave is generated by applying 55 Mhz, ~ msec. duration rf pulse to the interdigital transducer. The semiconductor is placed at the surface of the delay line as shown in Fig. 1b. The nonlinear acoustoelectric interaction, i.e., the interaction between the electric field of SAW and the free carriers of the semiconductor, results in the development of acoustoelectric voltages across the semiconductor [13]. The transverse and longitudinal components of the acoustoelectric voltage (TAV and LAV) are detected as shown in Fig. 1b. TAV spectroscopy is performed by illuminating the semiconductor surface, through the LiNbO₃ substrate, with monochromatic light (photon energy = E_{ph}). A lock-in amplifier, synchronized with SAW rf pulse, is used to detect acoustoelectric voltages and a x-y recorder is used to record the acoustoelectric voltage variation with temperature, SAW frequency and photon energy. Experiments involving the convolution voltages were performed by applying two

identical rf pulses to IDT's at the two ends of the LiNbO₃ delay line [14]. SAW generated by these pulses travel along the delay line and overlap beneath the semiconductor that is placed at the center of the delay line. The convolution signal is picked up across the semiconductor as shown in Fig. 1c. The semiconductor samples used in the present work were usually 1 cm x 1 cm (about 3.5 μsec long) and the input signals were rectangular pulses with 2 μsec duration. The convolution signal with 2 μsec duration (the usual time compressed waveform). To make sure that the triangular pulses are indeed the convolution signals, it was checked to see whether they disappear upon disconnection of either of the input signals.

i) Acoustoelectric voltage versus SAW frequency and temperature measurements

Figure 2 shows TAV versus SAW frequency of the superlattice and a bulk GaAs. The small variations in the TAV of GaAs can be attributed to the ripples in the frequency response of the interdigital transducer and there is no reversal of the polarity of the TAV as a function of SAW frequency. The TAV of the superlattice, on the other hand, exhibits drastic variation as a function of SAW frequency and the polarity of TAV changes from +ve to -ve within 10 KHz change in the SAW frequency (i.e., $\Delta f_{SAW} \sim 10$ KHz). The TAV becomes negative when the superlattice is illuminated by an above bandgap light ($E_{ph} \sim 1.5$ eV) and the strong dependence of the TAV on the SAW frequency diminishes [15]. Similar oscillations as a function of SAW frequency also have been observed in the longitudinal component [15,16] of the acoustoelectric voltage (LAV).

Figure 3 shows the temperature dependence of the LAV of the bulk semiconductor and the superlattice. It has been shown that the TAV and LAV of the bulk semiconductor, at dark, decreases monotonously as the temperature is decreased [17]. The LAV of the superlattice exhibits oscillation between +ve and -ve while its absolute magnitude decreases as the temperature is decreased. Similar oscillation as a function of temperature also occurs in TAV [15]. These oscillations in the acoustoelectric voltage of the superlattice diminishes when the sample is illuminated by an above the bandgap light (Fig. 3).

The above experimental observation can be summarized as follows: i) the acoustoelectric voltages of GaAs/AlAs superlattice exhibit strong variations as a function of SAW frequency ($\Delta f_{SAW} \sim 10$ KHz), ii) they also exhibit strong dependencies on temperature, iii) SAW power does not affect the behavior of the acoustoelectric voltages, it only changes their magnitude, and iv) these variations diminish when the superlattice is illuminated by a white light.

To explain the dramatic changes in the acoustoelectric voltages as a function of SAW frequency, the following mechanisms are considered: i) increase in the number of free electron concentration due to the induced transitions by ~ 55 Mhz electric field, and ii) the superlattice region behaves like a piezoelectric SAW delay line generating acousto-

electric voltage across the semi-insulating substrate.

It is not apparent how the ~ 55 Mhz electric field can induce transitions among different electronic levels ($\Delta E \sim 100$ meV). Also, the free electron density that should be present to produce the observed positive TAV magnitude is approximately around 10^{12} cm⁻³. The requirement of such a large magnitude of free electron density makes the first mechanism even less likely. It is conceivable, however, that the SAW in LiNbO₃ can generate elastic waves in the adjacent superlattice. Noting that LAV changes sign when the SAW direction is changed, and assuming that LAV contributes to the acoustoelectric voltage that is detected across the superlattice, the following argument can be given. At certain SAW frequencies, due to reversal of the velocity of elastic wave in the superlattice, the LAV changes sign reversing the sign of the acoustoelectric voltage that is detected across the semiconductor.

Another possibility related to the above mechanism, is the selective generation or transmission of the acoustic wave by the superlattice region. This is discussed in reference [18]. Also, it is conceivable that the superlattice is behaving as a vertical SAW transducer where the combination of the rectified voltage of this transducer and the acoustoelectric voltage determines the polarity of the detected signal. These discussions are only of qualitative nature and a more satisfactory SAW-superlattice interaction model is required to quantitatively explain the TAV behavior in superlattices.

ii) Acoustoelectric voltage spectroscopies

The experimental setup is identical to the one that is described in the beginning of the last section (Fig. 1) except that the x axis of the x-y recorder indicates the incident photon energy (or wavelength). The light is directed at the surface of the semiconductor through the LiNbO₃ delay line where the SAW-semiconductor interaction takes place (Fig. 1b). The electric field of the incident light is parallel to the 2D plane.

Figure 4 shows the TAV spectrum of a single MOCVD grown quantum well having Al_{0.3}Ga_{0.7}As(n⁺)/GaAs (200 Å) structure. Different structures at the high energy region ($E_{ph} > 1.4$ eV) of the spectrum are related to photoexcited electronic transitions in the semiconductor. These are discussed in the remainder of this section.

In bulk semiconductors and at SAW frequencies less than the dielectric relaxation frequencies [13,19] (i.e., $\omega_{SAW} < \omega_c$) the carrier conductivity dependence of the TAV polarity can be described as follows [13].

$$TAV \propto \frac{q\mu_n n - q\mu_p p}{q\mu_n n + q\mu_p p} \quad (1)$$

where n and p are, respectively, electron and hole concentrations and μ_n and μ_p are corresponding mobilities in the perpendicular direction of the SAW propagation plane. According to the above

equation, the TAV is positive for n-type semiconductors ($n > p$) and it is negative for p-type semiconductors ($p > n$).

The TAV spectroscopy [20] is similar to the photoconductivity measurements and since TAV has different polarity for electron and hole conductivities it is somewhat complicated and it goes through a maximum and a minimum as the electron conductivity is increased [13,19]. In the region where electron concentration changes between 10^{10} cm^{-3} in GaAs, the TAV is linear and it increases as the conductivity is increased. Assuming that all the other parameters are kept constant, any change in the TAV amplitude can be related to a change in carrier concentration and/or to the carrier mobility.

Based on the above considerations, different structures at the above bandgap region ($E_{ph} > E_g$) of the TAV spectrum shown in Fig. 4 can be related to the subband transitions [20]. The electronic transitions among the conduction and valence band sublevels theoretically should couple to a photon with an electric field perpendicular to the 2D plane. However, due to interface states, coupling to photons with electric fields parallel to the 2D planes have also been observed [21]. In some of these measurements it has been found that the 2D plane conductivity versus incident photon energy exhibits structures that can be related to sublevel transitions. These structures exist despite the fact that the number of photo-excited carriers are approximately kept constant in the quantum well. Lower electron mobility at higher energy levels might be responsible for the resonant photoconductivity in the 2D plane. Although this is not well understood, it has been attributed to the higher scattering rates that electrons experience at higher energy levels [21].

We are in the process of studying the exact mechanism of the acoustoelectric interaction in quantum wells and superlattices and at this stage a concise explanation of this interaction does not exist. However, assuming that the 2D plane conductivity also contributes to the TAV signal, the TAV spectrum shown in Fig. 4 can be explained as follows. The TAV amplitude at the above bandgap photon energy is much larger than its amplitude at dark and also the decay constant of the SAW electric field in high resistivity materials (the substrate is high resistivity) is approximately proportional to the inverse of the acoustic wave number which is around $10 \text{ } \mu\text{m}$ for 55 Mhz SAW.

Hence, there are two contributions to the TAV amplitude in the region where $E_{ph} > E_g$: a) the acoustoelectric interaction with the bulk carriers and b) the acoustoelectric interaction with the 2D plane carriers. When the photon energy is not equal to one of the sub-level transition energies, the signal due to the acoustoelectric interaction with the bulk carriers determines the amplitude of the acoustoelectric voltage. When the incident photon energy is equal to one of the sublevel transition energies, due to screening, the acoustoelectric interaction with the 2D plane carriers becomes relatively important. This results in a small reduction of the TAV.

Therefore the sublevel transitions correspond to valleys in the TAV spectrum and not to hills. Taking the quantum well width to be around 200 \AA and its height to be very large, the structures that are labeled in Figure 4 with letters A through G are identified with the following transitions. "A" is interface state to bulk conduction band transition. This is discussed in detail in ref. [11]. "B" is due to the large penetration depth of the around the bandgap energy ($E_{ph} \approx E_g$) photons into the bulk. "C" is due to the bound exciton formation in the bulk. This is discussed in detail in ref. [17]. "D" through "G" are due to the valence to conduction band sublevel transitions shown in the Fig. 4 inset. Also shown in Fig. 4 inset is a table that shows the calculated and experimental values of the transition energies. The agreement is better than one percent.

III. Convolution Voltage Measurements

Figures 5 to 7 show the convolution signals that are detected across bulk Si, bulk GaAs and GaAs/AlAs superlattices respectively. In bulk semiconductors the common feature of the convolution signals is that these shapes do not change when the SAW frequency is changed within the bandwidth of the IDT's. However, in the superlattice within 10 Khz change in the SAW frequency, few other triangular shaped satellite convolution pulses develop with a time delay near the original convolution pulse. An attempt is being made to time resolve these pulses and separate them from the regular convolution pulse. It is well known that if $f(t)$ and $g(t)$ are two signals that are respectively applied to the IDT's at both ends of the delay line, the voltage that is detected across the semiconductor is approximately given by [14]:

$$s(t) = \int_{t-L/v}^{t+L/v} f(\tau) g(2t-\tau) d\tau \triangleq f(t) * g(t) \Bigg|_{t \rightarrow 2t} \quad (2)$$

Now, if a slow (velocity = v_g) and a fast (velocity = v_f) SAW are generated corresponding to each input, input signals $f(t)$ and $g(t)$, two convolution signals will be developed across the semiconductor. It is clear that a slight time delay (t_d) will exist between these two convolution signals due to difference in the wave velocities. Also, it can be shown that t_d is given by

$$t_d = d \left(\frac{1}{v_s} - \frac{1}{v_f} \right) \quad (3)$$

$2d$ is the length of the superlattice as also the length of the interaction region. Of course, due to the spatial dependence of the second order signals that result from the contribution of contra-directed fast and slow waves, they should also be considered.

Based on the above consideration it is reasonable to assume that slow waves generated in the superlattice are responsible for the development of the satellite convolution signals. Taking t_d to be around $1.6 \text{ } \mu\text{sec}$ from Fig. 7a, d to be around

0.5 cm (here d is half the length of the semiconductor) and v_f to be 348800 cm/sec (velocity of SAW on the y cut z propagating LiNbO_3) v_s is found from equation (3) to be around 1.7×10^5 cm/sec. This is an order of magnitude larger than the value of v_s that is calculated from TAV versus f_{SAW} graph ($v_s = \Delta f \times 1 \text{ cm} = 10 \text{ Khz} \times 1 \text{ cm} = 10^4 \text{ cm/sec}$) [15].

Thus it appears that generation of slow waves in superlattice due to the passage of the SAW on the LiNbO_3 is responsible for the experimentally observed oscillations in TAV versus SAW frequency curves and the appearance of the satellite convolution signals in superlattices. Why the generation, or why the strength of generation of these slow waves depend on the exciting SAW frequency is yet an open question. However, due to the highly dispersive nature of layered structures, it is not surprising to observe such a frequency dependency in superlattices [22].

The above results and observations clearly show the potential of SAW technique in nondestructive evaluation of superlattices. Also, the rich phenomena that occur as a result of SAW-superlattice interaction may be used in SAW based devices such as frequency discrimination and frequency controlled switches.

ACKNOWLEDGEMENT - It is a pleasure to acknowledge the samples used in this experiment were provided by Varian Research Center, Palo Alto, CA and Dr. Ayub Fathimulla of Allied-Bendix Aerospace Technology Center, Columbia, MD.

REFERENCES

1. J. Chevier and D. Delagebeaudeuf, Two-Dimensional Systems: Physics and New Devices, Editors: G. Bauer, F. Kuchar and H. Heinrich, Springer-Verlag, New York, pp. 250-259 (1986).
2. T.C.L.G. Sollner, E.R. Brown, W.D. Goodhue and H.Q. Le, Appl. Phys. Lett., 50(6), pp. 332-334.
3. R.G. Wheeler and H.S. Goldberg, IEEE Trans. on Electron Devices, Vol. ED-22, pp. 1001-1009
4. F. Capasso, S. Sen, A.Y. Cho and D. Sivco, IEEE Electron Device Lett., Vol. EDL 8(7), pp. 297-299 (1987).
5. A. Harwit and J.S. Harris, Appl. Phys. Lett. 50(11), pp. 685-687 (1987).
6. R. Dingle, A.C. Gossard and W. Wiegmann, Phys. Rev. Lett., Vol. 34, pp. 1327-1330 (1975).
7. A.C. Gossard, IEEE Trans. on Electron Devices, Vol. ED-21(11), pp. 1662-1667 (1984).
8. Amitava Chatterjee, Pankaj K. Das and Laurence B. Milstein, IEEE Trans. Sonics and Ultrasonics, Vol. SU-32, pp. 745-759 (1985).
9. R. L. Gunshor, Solid State Electron., Vol. 18, pp. 1089-1093 (1975).
10. M. Hoskins, F. Fliegel, S. Mahon, S. Datta and B.J. Hunsinger, 1980 IEEE Ultrasonics Symposium Proceedings, Pub. No. 88CH1602-2, Vol. 1, pp. 142 (1980).
11. M. Tabib-Azar and P. Das, IEEE Ultrasonics Symposium Proc., IEEE Pub. No. 85CH2209, pp. 1016-1021 (1985).
12. A. Wixforth, J. Pokotthaus and G. Weimann, Phys. Rev. Lett. 56, 2104 (1986).
13. P. Das, M.K. Roy, R.T. Webster and K. Varahramyan, Proc. IEEE Ultrasonics Symp., pp. 278 (1979).
14. E.A. Ash, "Fundamentals of Signal Processing Devices" in Topics in Applied Physics, edited by A.A. Oliner, Springer-Verlag, New York, NY (1978).
15. M. Tabib-Azar and P. Das, Appl. Phys. Lett., 51(6), pp. 436-438 (1987).
16. A. Bers, J.H. Cafarella and B.E. Burke, Appl. Phys. Lett., Vol. 22, pp. 399 (1973).
17. M. Tabib-Azar and P. Das, J. Appl. Phys., to be published.
18. Narayanamurti, H. Halstormer, M.A.G. Chin, A.C. Gossard and W. Wiegmann, Phys. Rev. Lett. 27, 2012 (1979).
19. I.J. Fritz, J. Appl. Phys. 52(11), 6749 (1981).
20. M.N. Abedin, P. Das and A. Fathimulla, Superlattices and Microstructures, to be published.
21. D.C. Rogers and R.J. Nicholas, J. Phys. C, Vol. 18, pp. L891-896 (1987).
22. F. Palma and P. Das, Ultrasonic Symposium Proceedings, IEEE Pub. No. 0090-5607/86, pp. 457-461 (1986).

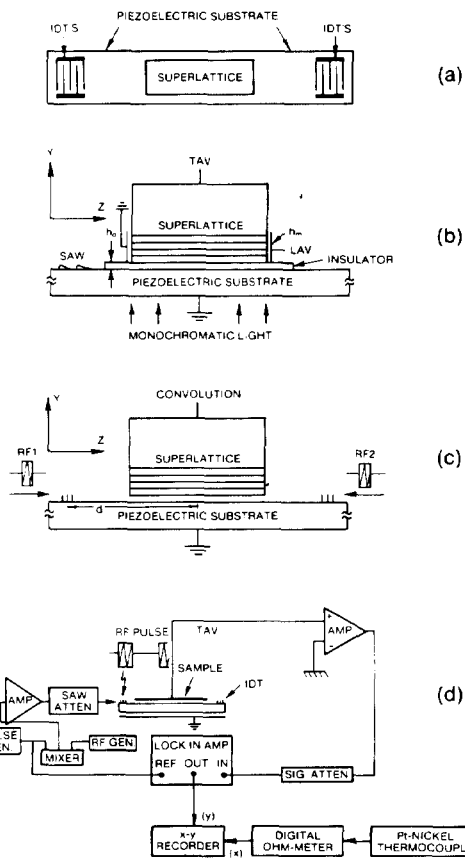


Fig. 1 The delay line is shown in (a), different acoustoelectric voltages are shown in (b) and (c) and the experimental setup is shown in (d).

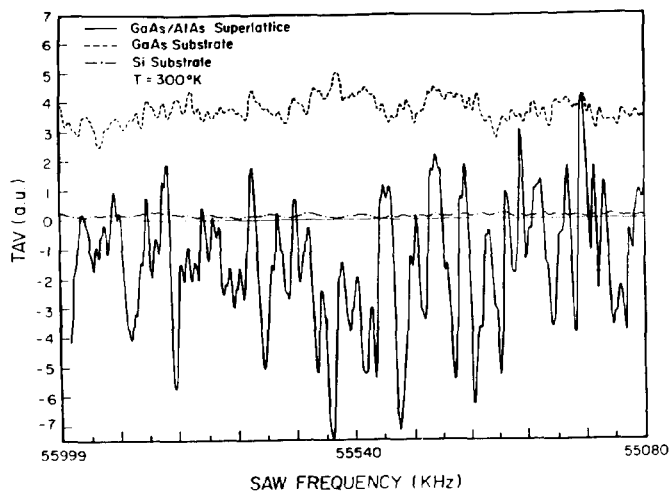


Fig. 2 TAV versus SAW frequency ($TAV-f_{SAW}$) of the GaAs/AlAs at dark. The $TAV-f_{SAW}$ of GaAs substrate (dashed line) at dark.

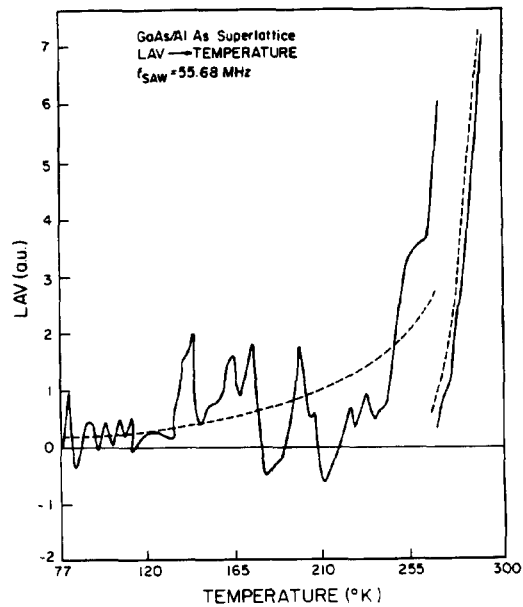


Fig. 3 LAV versus temperature of the GaAs/AlAs superlattice at dark (solid line) and under illumination (dashed line).

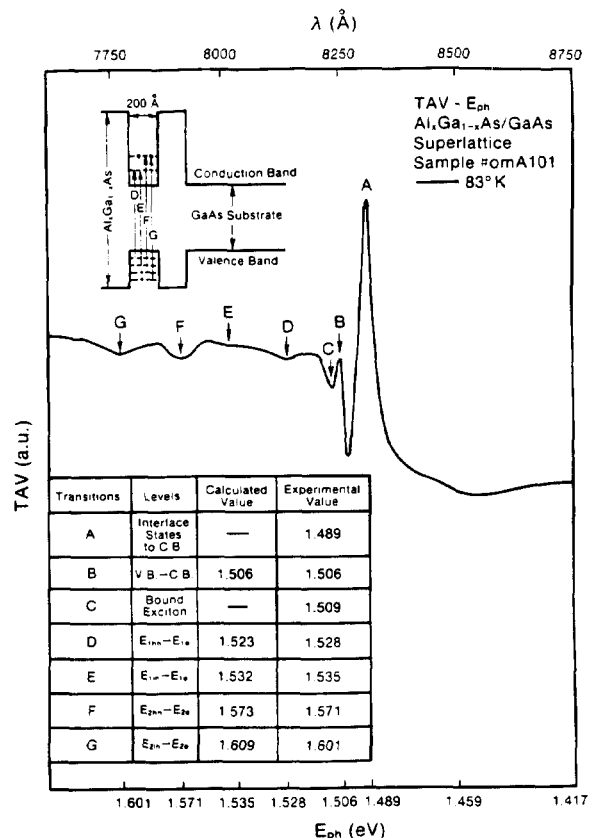
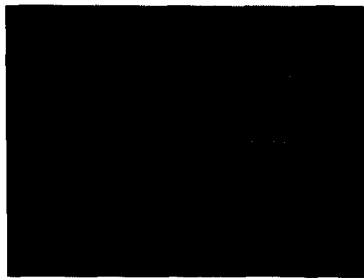
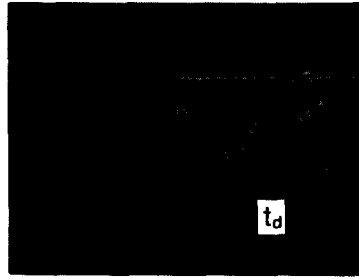


Fig. 4 TAV spectrum of AlGaAs/GaAs quantum well at 83 K.



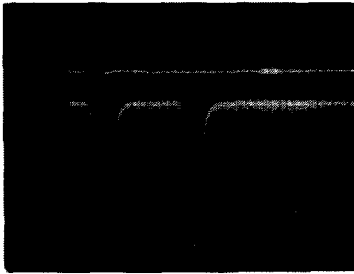
Trace (1)

Trace (2)



Trace (1)

Trace (2)



Trace (1)

Trace (2)



Trace (1)

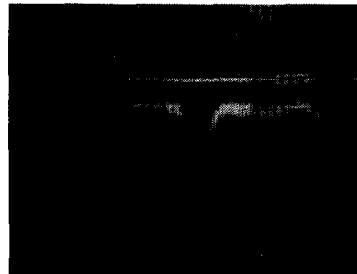
Trace (2)

Fig. 5 Trace (1): the rf pulse applied to IDT's, Trace (2): convolution voltage across an n-type silicon. a) $f_{SAW} = 55$ Mhz, b) $f_{SAW} = 55.76$ Mhz, horizontal scale: $2 \mu s/div.$, vertical scale: rf pulse $lv/div.$, convolution voltage $lv/div.$



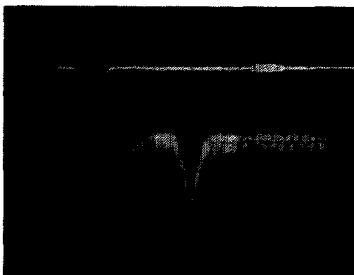
Trace (1)

Trace (2)



Trace (1)

Trace (2)



Trace (1)

Trace (2)

Fig. 7 Trace (1): the rf pulse applied to IDT's, Trace (2): convolution voltage across a GaAs/AlAs superlattice. a) $f_{SAW} = 55.41$ Mhz, b) $f_{SAW} = 55.35$ Mhz, c) $f_{SAW} = 55.74$ Mhz, horizontal scale: $2 \mu s/div.$, vertical scale: rf pulse $2v/div.$, convolution voltage $lv/div.$

Fig. 6 Trace (1): the rf pulse applied to IDT's, Trace (2): convolution voltage across a high resistivity GaAs (Cr doped). a) $f_{SAW} = 55$ Mhz, b) $f_{SAW} = 55.36$ Mhz, horizontal scale: $2 \mu s/div.$, vertical scale: rf pulse $5v/div.$, convolution voltage $0.5v/div.$